Acta Biomaterialia 9 (2013) 7326–7334

Contents lists available at SciVerse ScienceDirect

Acta Biomaterialia

journal homepage: www.elsevier.com/locate/actabiomat

Failure mechanisms in fibrous scaffolds

C.T. Koh [a,b], D.G.T. Strange [a], K. Tonsomboon [a], M.L. Oyen [a,*]

[a] Cambridge University Engineering Department, Trumpington Street, Cambridge CB2 1PZ, UK
[b] Faculty of Mechanical and Manufacturing Engineering, Universiti Tun Hussein Onn Malaysia, 81310 Parit Raja, Johor, Malaysia

ARTICLE INFO

Article history:
Received 21 November 2012
Received in revised form 24 February 2013
Accepted 26 February 2013
Available online 5 March 2013

Keywords:
Fibrous networks
Toughening mechanisms
Fracture
Electrospun scaffolds
Nonwoven

ABSTRACT

Polymeric fibrous scaffolds have been considered as replacements for load-bearing soft tissues, because of their ability to mimic the microstructure of natural tissues. Poor toughness of fibrous materials results in failure, which is an issue of importance to both engineering and medical practice. The toughness of fibrous materials depends on the ability of the microstructure to develop toughening mechanisms. However, such toughening mechanisms are still not well understood, because the detailed evolution at the microscopic level is difficult to visualize. A novel and simple method was developed, namely, a sample-taping technique, to examine the detailed failure mechanisms of fibrous microstructures. This technique was compared with in situ fracture testing by scanning electron microscopy. Examination of three types of fibrous networks showed that two different failure modes occurred in fibrous scaffolds. For brittle cracking in gelatin electrospun scaffolds, the random network morphology around the crack tip remained during crack propagation. For ductile failure in polycaprolactone electrospun scaffolds and nonwoven fabrics, the random network deformed via fiber rearrangement, and a large number of fiber bundles formed across the region in front of the notch tip. These fiber bundles not only accommodated mechanical strain, but also resisted crack propagation and thus toughened the fibrous scaffolds. Such understanding provides insight for the production of fibrous materials with enhanced toughness.

1. Introduction

Polymeric fibrous scaffolds have been studied extensively, owing to their promise as tissue engineering scaffolds for load-bearing soft tissues [10] such as the annulus fibrosus of the intervertebral disc [2], cartilage, blood vessels [4] and amniotic membrane [5]. Their material structure mimics the hierarchical structure of load-bearing soft tissues at three levels: polymer chains in a single fiber at a molecular scale; fibrous networks at a microscopic scale; and bulk membranes at a macroscopic scale.

The characteristics of microscopic fibrous network architecture such as fiber orientation [6], fiber density [7] and cross-link density [8] influence the deformation properties of the material. Through an understanding of the relationship between microstructural features and deformation, useful guidelines can be provided to reproduce various aspects of mechanical behavior for tissue engineering. For instance, highly anisotropic materials with similar tensile stiffness to annulus fibrosus have been produced by controlling fiber orientation [2], and other fibrous networks approaching the biaxial stiffness of blood vessels have been reproduced by mimicking the network, with fibers aligning in the helical direction [9].

An understanding of failure mechanisms is crucial in the study of fracture [10]. The toughness of a material depends on the ability of the microstructure to dissipate energy without propagation of a crack. Therefore, an understanding of the failure mechanisms presented in fibrous networks can provide insights into the production of tissue-engineering scaffolds with improved toughness. It also provides basic physical understanding of structural failure in diseases and conditions that involve soft tissue failure.

The incomplete knowledge of toughening mechanisms in fibrous networks is due to fact that the microstructure evolution during failure process is difficult to visualize. Current imaging techniques such as small angle light scattering (SALS) [16,17], polarized light microscopy [18], confocal microscopy and digital image correlation [19] have been used to characterize microstructural morphology, including the fiber distribution. There are two limitations to these studies. First, the detailed microstructural fibrous network features, including fiber diameter and network bonding, are hard to see. For instance, mean scattered light distribution identifies fiber orientation, but is unable to show detail at the level of an individual fiber. Second, it is difficult to maintain the deformed configuration of the microstructure during visualization, and special apparatus is needed to fit within imaging tools to stretch the sample in situ.

The objective of the work presented here is to examine the failure mechanisms of fibrous scaffolds at both macroscopic and

* Corresponding author.
E-mail address: mlo29@cam.ac.uk (M.L. Oyen).

1742-7061/$ - see front matter © 2013 Acta Materialia Inc. Published by Elsevier Ltd. All rights reserved.
http://dx.doi.org/10.1016/j.actbio.2013.02.046

microscopic scales. Uniaxial tensile tests and fracture tests were first performed. The detailed toughening mechanisms at the notch front were then examined by scanning electron microscopy (SEM) and optical microscopy. A novel and simple method, namely a sample-taping technique, was developed to capture the deformed microstructures by SEM. Further, in situ fracture testing by SEM was also performed to compare with the sample-taping technique. This study provides a basic understanding of the toughening mechanisms present in fibrous networks, by considering the non-linear and non-affine deformation of the fibers present in the network. Such understanding facilitates the production of engineering fibrous materials with enhanced toughness.

2. Method

2.1. Sample preparation

The three types of polymeric fibrous scaffolds studied in this paper are gelatin electrospun scaffolds, polycaprolactone (PCL) electrospun scaffolds and nonwoven fabrics; these three materials have different material length scales and network properties. Gelatin, PCL and nonwoven fibers have diameters of ~80 nm, 1and 20 μm, respectively. The undeformed scaffolds of both gelatin and PCL electrospun scaffolds are random networks, while the undeformed nonwoven fabric is slightly oriented. The thicknesses of all scaffolds were determined using digital calipers and were taken as the mean thickness of eight individual measurements; the thicknesses of gelatin electrospun scaffolds, PCL electrospun scaffolds and nonwoven fabrics were 0.20 ± 0.03, 0.39 ± 0.05, 0.48 ± 0.05 mm respectively.

Both gelatin and PCL electrospun scaffolds were produced by an electrospinning technique. The electrospinning apparatus consisted of a 20 ml syringe pump (KR Analytical Ltd., Sandback, UK) and a high-voltage power supply (Glassman High Voltage, Bramley, UK) to pull nano- to micrometer fibers from the polymer solution. An earthed 6-cm-diameter copper plate wrapped in aluminum foil was used as a collector. All chemicals used to create the electrospun scaffolds were purchased from Sigma Aldrich (Dorset, UK).

The gelatin electrospun fibers were created following a method developed by Song et al. [20]. A 10 wt.% gelatin solution was prepared by dissolving 10 g of gelatin from porcine skin (250 g bloom strength) in a water-based co-solvent composed of 42 g of glacial acetic acid, 21 g of ethyl acetate and 10 g of distilled water. The solution was stirred for 2 h at room temperature and further incubated for 30 min at 50 °C. The gelatin solution was loaded into a plastic syringe, which was placed 10 cm vertically to the earthed collector. The solution was then pumped through a blunt 18G needle at 0.003 ml min^{-1}. An applied voltage of 12 kV was applied. The gelatin electrospun mats were collected after 6 h and dried in a desiccator for 24 h to remove residual solvent.

The PCL electrospun fibrous networks were created following a similar method to that of Li et al. [21]. A 14% w/v solution of PCL (80,000 g mol^{-1}) in a 1:1 mixture of dimethylformamide and tetrahydrofuran was prepared. The solution was pumped through a blunt needle at 0.007 ml min^{-1}, using a syringe pump. Either 18 or 19 G needles were used. The needle was mounted vertically 20 cm above an earthed 6-cm-diameter copper plate wrapped in aluminum foil. A voltage of 12 kV was applied between the needle and the copper plate. The resultant fiber mat was collected from the aluminum foil after ~1 h of electrospinning.

Nonwoven fabrics studied in this paper were 14 gsm carded polypropylene/polyethylene fabric (Fiberweb Corovin GmbH, Peine, Germany). The fibers were bonded using an air through-bonding technique.

2.2. Uniaxial and fracture tests

Uniaxial and fracture tests were performed on an Instron 5544 universal testing frame (Canton, MA, USA) with a 500 N load cell. All samples were deformed at a constant rate of 0.05 mm s^{-1}. Samples were slightly slack at the beginning of the test to prevent application of pre-stress in the samples before the tests. The first displacement when the force was greater than 0.005 N was used as the reference for zero displacement. Small colored markers were added to the sample surfaces to show local displacements. Deformation was observed by comparing either the distance between the adjacent markers or the change in shape of the elliptical markers. A Pixelink PL-B776F camera (Ottawa, Canada) or JVC Everio GZ-NG330 camcorder was used to capture pictures every second during the fracture tests.

The uniaxial test samples were cut based on the size of the loaded section of the fracture test: they have the same length, the width of uniaxial sample is equal to the width of fracture sample minus the notch length, and the notch length was one-third of the sample width. Using this geometry, the crack sensitivity can be qualitatively studied by comparing the force–displacement curves. The gelatin electrospun scaffolds were cut to 3.5×20 mm for fracture and 5×20 mm for uniaxial tests, the PCL electrospun scaffolds were cut to 3.818×7 mm for fracture and 2.5×7 mm for uniaxial tests, and the nonwoven fabrics were cut to 6×11 mm for fracture and 4×11 mm for uniaxial tests. Five to six samples were cut for both uniaxial and fracture tests for all materials.

2.3. Microstructure visualization

The deformation of microstructures was visualized using two methods, a novel sample-taping technique and an in situ fracture test technique, as illustrated in Fig. 1. In the sample-taping technique, the scaffolds were first stretched to the assigned engineering strain ε on an Instron 5544 universal testing frame (Canton, MA) with a 500 N load cell. Three applied strains were used to examine the local microstructure near small, medium and large notch openings, as illustrated in Fig. 1b. Both the small and medium notch opening samples were from before the force started to decrease, while the large notch opening sample was from after the force started decreasing. The deformed samples were then fixed to adhesive carbon discs. These taped samples were visualized by either SEM or optical microscopy. The samples were coated with gold prior to SEM visualization under high vacuum. It was verified that the load–displacement responses for these samples were the same as those tested to failure, to within experimental variability. In the in situ fracture test technique, the uncoated scaffolds were pulled using a custom-built tensile test device in the SEM instrument. Images of the deformed microstructures were captured at every small increment of strain in an environmental mode.

Both gelatin and PCL electrospun scaffolds were visualized in an FEI Philips (UK) XL30 field emission gun scanning electron microscope equipped with an Oxford Instruments (UK) INCA EDX system. The gelatin electrospun scaffolds were visualized using only the sample-taping technique. The engineering strain $\varepsilon = 6\%$ was assigned, as this was when the crack started propagating. The PCL electrospun scaffolds were visualized using both techniques. For the sample-taping technique, the three assigned strains corresponding to small, medium and large notch openings were $\varepsilon = 29\%$, 65% and 135%. For the in situ fracture test technique, the deformed microstructures were captured every 7% strain.

The nonwoven fabrics have a larger material length scale, and their microstructures were visualized in an optical microscope. A similar sample-taping method was used to visualize the nonwoven fabrics. The assigned engineering strains ε were 14%, 27% and 55%,

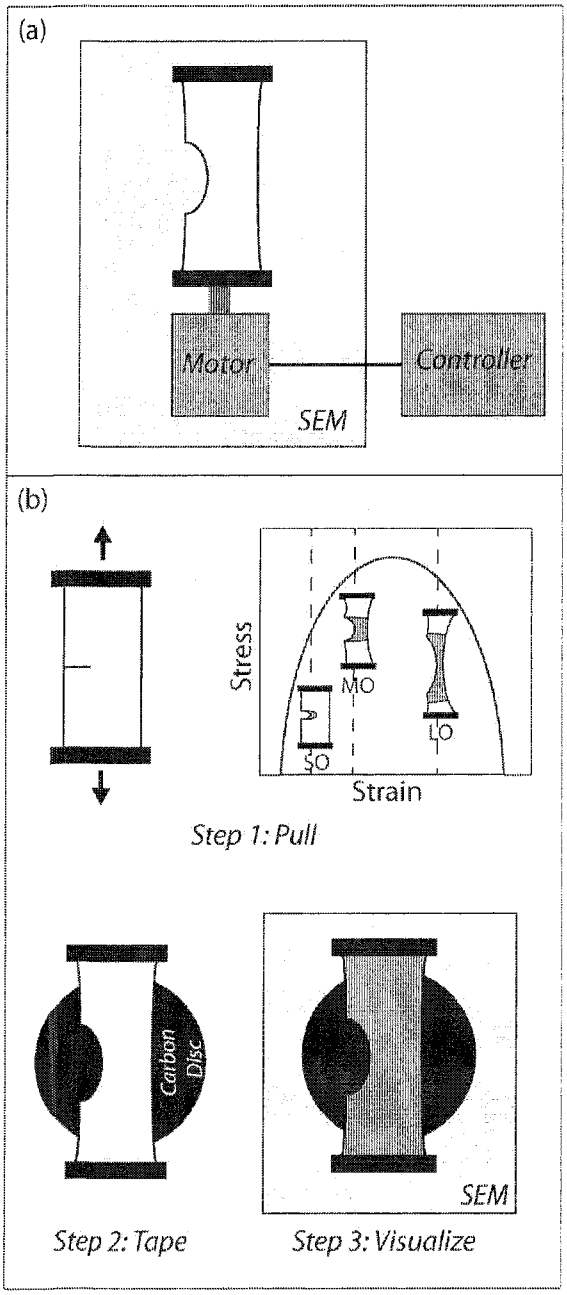

Fig. 1. Schematic illustration of (a) an in situ fracture test and (b) a sample-taping technique. Step one involves pulling the fracture sample to assigned strain to examine the crack at the small opening (SO), medium opening (MO) and large opening (LO). Step two involves fixing the deformed samples to the carbon disc. Step three involves visualizing the gold-coated sample by SEM.

referring to the small, medium and large notch openings, respectively.

2.4. Quantitative analysis of microstructure images

The microstructure images were analyzed using ImageJ [22,23] to quantify the network morphology, including fiber alignment and fiber diameter. Gelatin fiber alignment was obtained from a $41 \times 61\ \mu m^2$ region. The PCL fiber alignment was obtained from a $325 \times 500\ \mu m^2$ region in the vicinity of the notch tip. A region size of $4.1 \times 5.4\ mm^2$ was used to characterize alignment of nonwoven fabrics. A smaller area of microstructure, i.e. $10 \times 10\ \mu m^2$ was analyzed to obtain the fiber diameter of PCL scaffolds, using ImageJ.

3. Results

3.1. Toughening at macroscopic scales

During fracture tests, cracks in electrospun gelatin remained small (Fig. 2). Once cracks propagated, the samples broke within 1 s (an increase in strain $\Delta\varepsilon = 0.25\%$). The small red markers on the samples show qualitatively the local deformation of the material. From examination of the markers on samples corresponding to an increasing strain, little vertical deformation occurred.

Notches in PCL electrospun scaffolds and nonwoven fabrics blunted instead of propagating (Fig. 2) during fracture tests. By comparing the markers on the samples corresponding to an increasing strain, large vertical deformation occurred in both scaffolds. Further, the width of the front-tip region decreased more significantly than the vertical deformation in both scaffolds. The PCL electrospun scaffolds have large local deformations around the notch tip compared with the rest of the sample area. Nonwoven fabrics show more uniformly distributed local deformation throughout the sample.

Fig. 3 shows the comparison of force–displacement responses from between uniaxial and fracture tests. The nonwoven fabrics have similar curve trends, peak forces and failure displacements for uniaxial and notched fracture tests. In contrast, both gelatin and PCL electrospun scaffolds have different trends for uniaxial and notched fracture tests; the notched fracture curves exhibit smaller failure displacements than the curves from the unnotched uniaxial tests.

3.2. Toughening at microscopic scales

Fig. 4 shows the SEM images of the deformed fibrous networks in the vicinity of the notch tip of gelatin electrospun scaffolds, as obtained by the sample-taping technique. This deformed fibrous network was visualized when the crack started propagating. The undeformed scaffold was a random network, and the network remained random during crack propagation. Moreover, broken fibers were observed along the crack path.

Fig. 5 shows the SEM images of the deformed fibrous networks in the vicinity of the notch tip of a PCL electrospun scaffold, obtained by the in situ fracture test technique. The undeformed scaffold was a random network. This random network reoriented to become an aligned network under the applied loading. The preferred fiber direction was parallel to the loading direction and perpendicular to the notch tip. Moreover, a region of parallel fiber bundles formed in the vicinity of notch tip during small notch openings (strain $\varepsilon = 29\%$). As the sample was further pulled, it formed a blunted notch (strain $\varepsilon = 65\%$), and the size of the parallel fiber bundle region increased until it spanned approximately half the sample width. When the crack started propagating at 135% strain, the parallel fiber bundles had formed across the entire sample. A detailed tracking of individual fibers at the notch tip, as shown in the large magnification images, indicates some fiber ruptures at the notch tip.

Fig. 6 shows SEM images of the deformed fibrous networks in PCL electrospun scaffolds and microscope images of nonwoven fabrics, both obtained by the sample-taping technique. The same damage mechanism is found in the PCL electrospun scaffold, as observed in both the in situ fracture test technique and the sample-taping technique; parallel fiber bundles formed in the vicinity of the notch tip, and more bundles formed when the strain increased. The sample-taping technique produced clearer images compared

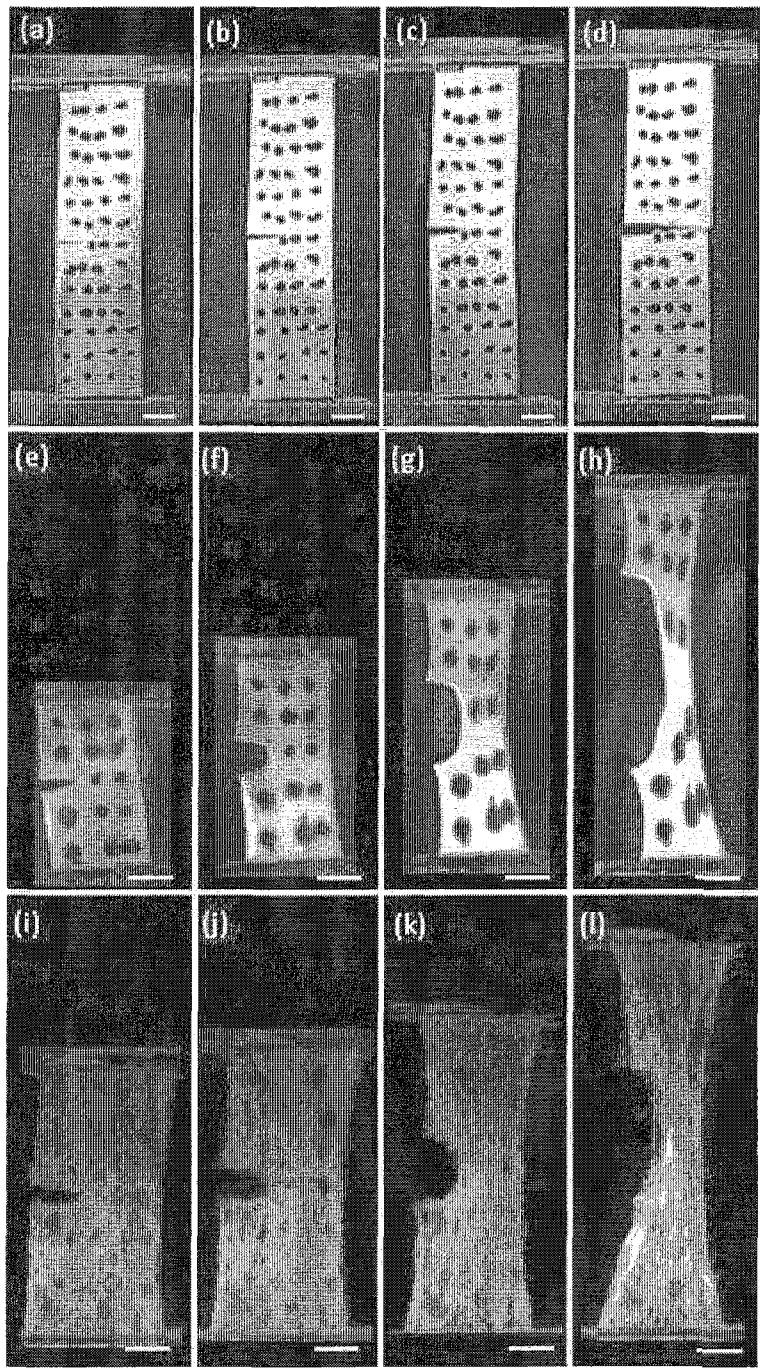

Fig. 2. Notch opening in fracture tests. (a–d) A gelatin electrospun scaffold was deformed to strains (a) $\varepsilon = 0$, (b) $\varepsilon = 2.6\%$, (c) $\varepsilon = 5.1\%$ and (d) $\varepsilon = 5.39\%$; (e–h) a PCL electrospun scaffold was deformed to strains (e) $\varepsilon = 9\%$, (f) $\varepsilon = 29\%$, (g) $\varepsilon = 65\%$ and (h) $\varepsilon = 135\%$; (i–l) a nonwoven fabric was deformed to strains (i) $\varepsilon = 7\%$, (j) $\varepsilon = 14\%$, (k) $\varepsilon = 27\%$ and (l) $\varepsilon = 55\%$. All scale bars represent 2 mm in length.

with the in situ technique, and the individual PCL fibers were clearly observed. Comparing the undeformed and deformed PCL network, it is apparent that not all intersection points between PCL fibers were bonded, allowing the PCL network to reorient to form parallel fiber bundles. Furthermore, those PCL fibers reoriented perpendicular to the applied loading buckled at 65% strain and broke at 135% strain.

The undeformed nonwoven fabric was an oriented fibrous network. The preferred fiber direction of the undeformed network was parallel to the loading direction and perpendicular to the notch tip. Similarly to the PCL electrospun scaffolds, when the samples were stretched, more fibers oriented to align parallel to the notch tip. Moreover, fiber bundles formed in all regions ahead of the crack tip, prior to crack propagation. However, the distribution of fiber bundles is different between PCL electrospun scaffolds and nonwoven fabrics, as illustrated in Fig. 7. The PCL electrospun scaffolds had an uneven distribution of fiber bundles; fiber bundles first formed in the vicinity of notch tip. Unlike the PCL electrospun scaffolds, the fiber bundles were uniformly distributed in the nonwoven fabrics.

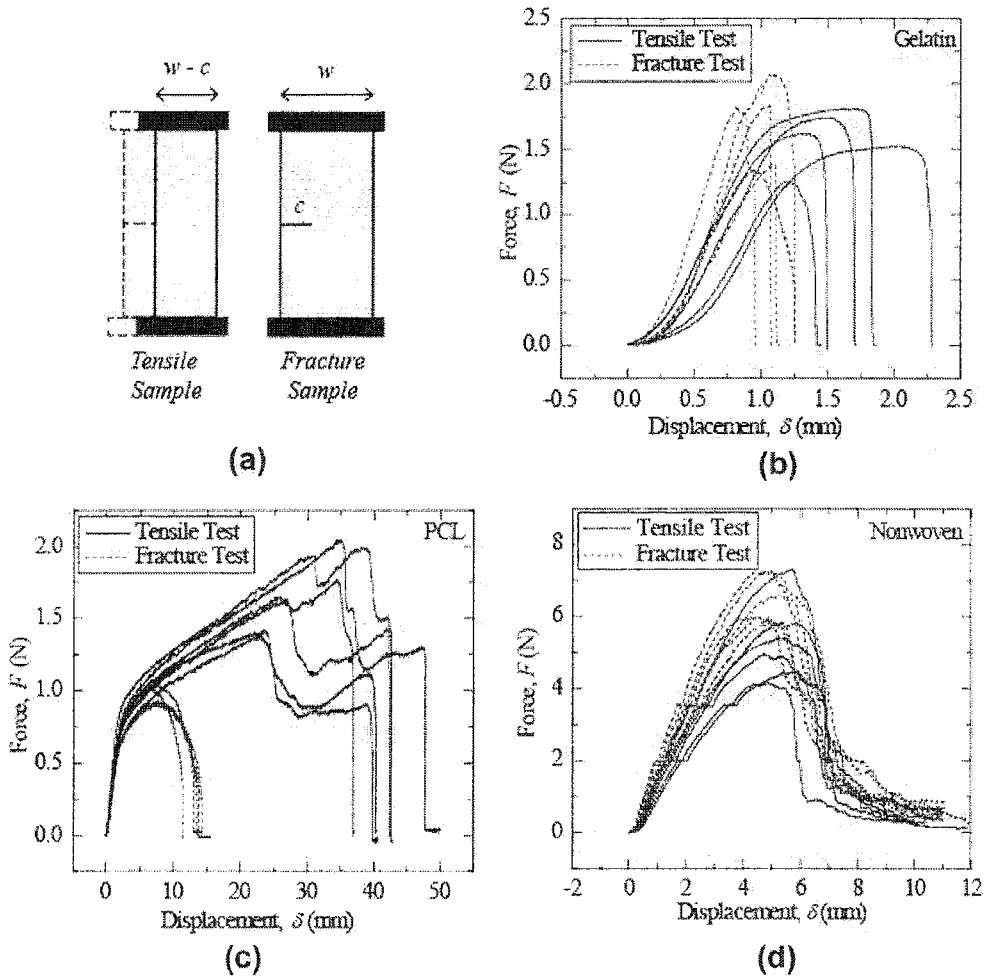

Fig. 3. (a) Sample geometries for tensile and fracture tests. (b–d) Force–displacement curves of uniaxial and fracture tests for (b) gelatin electrospun scaffolds, (c) PCL electrospun scaffolds and (d) nonwoven fabric samples.

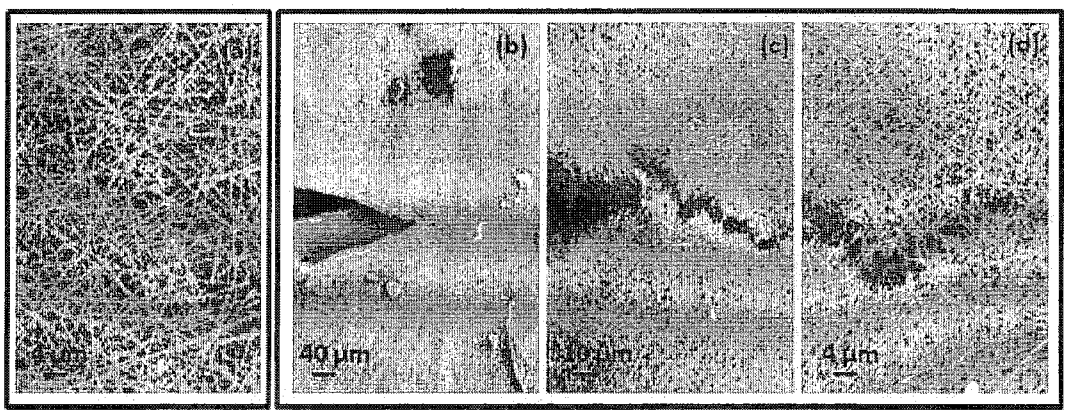

Fig. 4. SEM images of (a) undeformed and (b–d) deformed fibrous networks in the vicinity of the notch tip in gelatin electrospun scaffolds, captured by the sample-taping technique. The strain ε in images (b–d) was 6%.

3.3. Quantitative analysis

The fiber reorientation, which was captured by the sample-taping technique (Fig. 6), was quantified in ImageJ (Fig. 8). The angle 90° was for fibers that were aligned parallel to the notch tip, while angles 0° and 180° were for fibers aligned perpendicular to the notch tip. The gelatin fibers were initially random and remained random when strain increased, confirming that there was no fiber bundle formation during failure of gelatin, as shown in Figs. 4 and 7b. The PCL fibers were initially random, and the proportion of parallel fibers increased when the strain increased. The nonwoven fibers were initially not random; the undeformed network consists

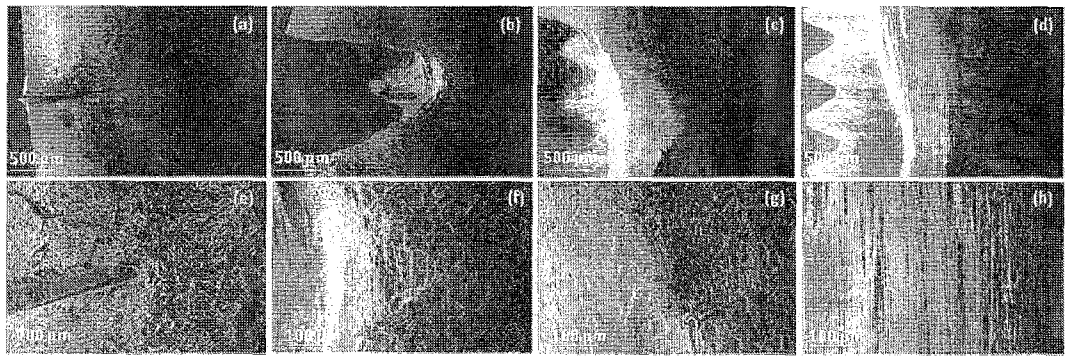

Fig. 5. SEM images of deformed fibrous networks in the vicinity of the notch tip of PCL electrospun scaffolds, performed by an in situ fracture test. The PCL electrospun scaffold was (a and e) undeformed and deformed by strains (b and f) $\varepsilon = 29\%$, (c and g) $\varepsilon = 65\%$ and (d and h) $\varepsilon = 135\%$ at 500 × and 1000× magnifications, respectively. The image background contains a screw from the in situ test device.

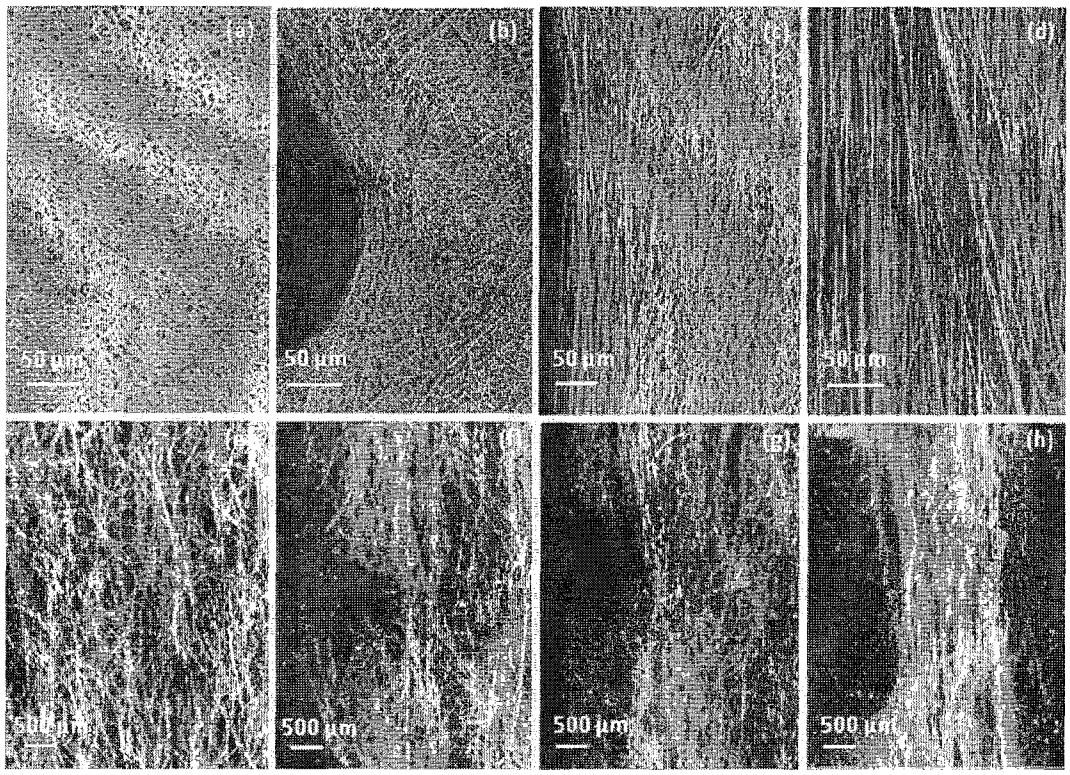

Fig. 6. The deformed fibrous networks in the vicinity of the notch tip, as captured by the sample-taping technique: SEM images are presented for (a–d) PCL electrospun scaffolds and optical microscopy images for (e, f) nonwoven fabrics. A PCL electrospun scaffold was (a) undeformed and deformed by strains (b) $\varepsilon = 29\%$, (c) $\varepsilon = 65\%$ and (d) $\varepsilon = 135\%$; a nonwoven fabric was (e) undeformed and deformed by strains (f) $\varepsilon = 14\%$, (g) $\varepsilon = 27\%$ and (h) $\varepsilon = 55\%$.

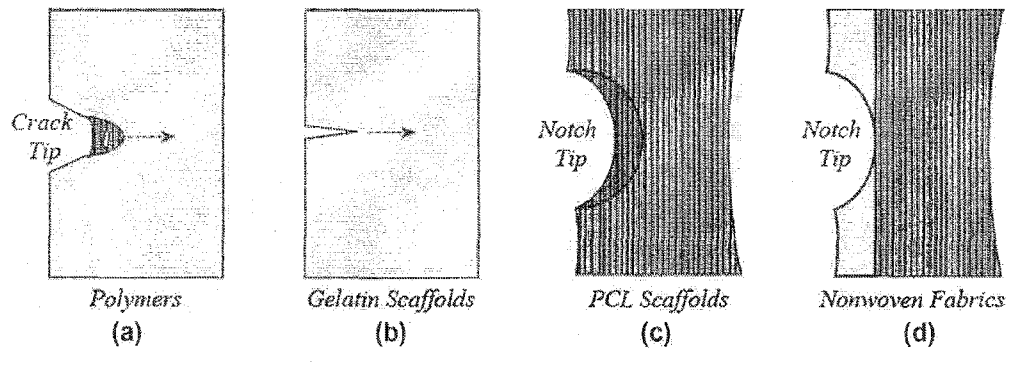

Fig. 7. Schematic illustration of failure mechanisms in (a) polymers, (b) gelatin electrospun scaffolds, (c) PCL electrospun scaffolds and (d) nonwoven fabrics.

of some fibers aligned parallel to the notch tip. Similar to the PCL networks, the proportion of parallel fibers increased as the displacement increased. Both materials demonstrated a reduced dispersion of fiber orientation when strain increased. The quantitative analysis of increasingly parallel fibers was consistent with the microscopic observations in Figs. 6 and 7c and d, and the fiber bundles were parallel to the crack tip.

The fiber diameters for fiber bundles formed in the PCL electrospun scaffolds were quantified (Fig. 9) from the SEM images of the fiber bundles at the notch tip at 20,000× magnification. There was substantial variation in fiber diameter, so it was unclear whether the fiber diameter changed when the strain increased.

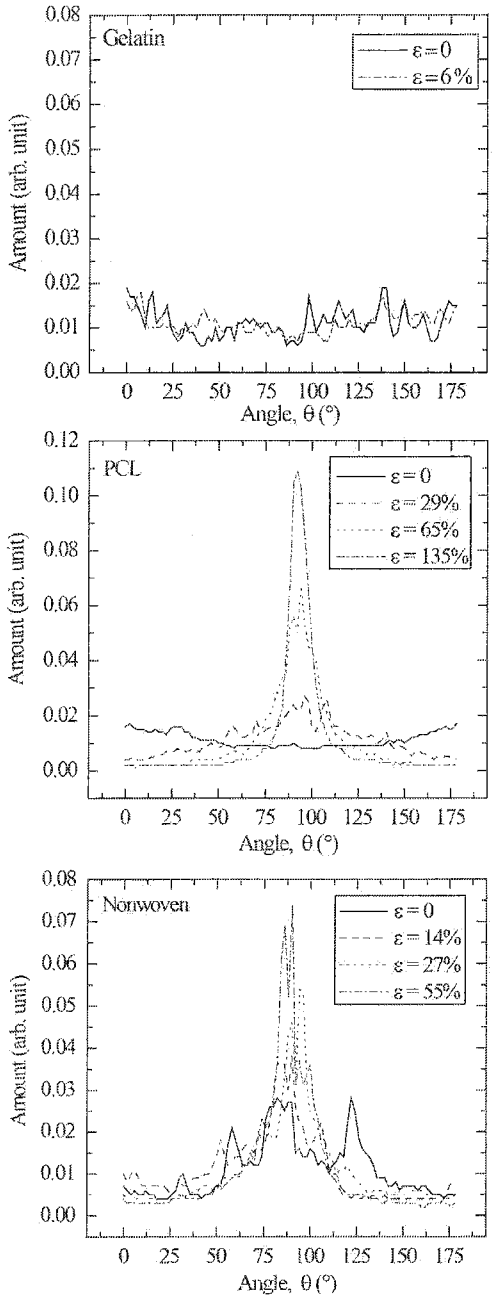

Fig. 8. Fiber realignment in gelatin electrospun scaffold, PCL electrospun scaffolds and nonwoven fabric in fracture tests as a function of increasing strain.

4. Discussion

4.1. Visualization techniques

A novel visualization technique, namely a sample-taping technique, was developed to visualize the deformation of fibrous microstructures. This technique is based on the assumption that the random morphology of undeformed fibrous scaffolds is consistent across samples. Instead of stretching one sample in an imaging device, multiple samples were stretched to the assigned single strains. Their deformation configurations were retained by adhesive tape prior to visualization. The sample-taping technique is simpler, quicker and cheaper compared with an in situ fracture technique, but at the same time it accurately captures the deformation condition of fibrous microstructures.

While an in situ fracture technique has been used extensively because of its ability to track deformation of a microstructure, three possible limitations of the in situ fracture test in a SEM were identified. First, the sample size of the in situ fracture technique is constrained by the limited space inside an SEM chamber. However, the fracture of most materials is sensitive to sample geometry. Second, many electrons are shot directly at the same region—the crack tip—every time the image is refocused. This repeated electron exposure may result in broken fibers. As a result, it is uncertain whether the broken fibers observed in the SEM are caused by failure mechanisms in the material or whether they were destroyed by the electron beam. Third, because the thin gold coating may affect the material deformation, the in situ test is performed on uncoated samples in environment mode, but the quality of the images taken in environment mode is poorer than that of gold-coated samples. The sample-taping technique overcomes all three of these limitations.

4.2. Brittle vs. ductile failure in fibrous materials

The detailed failure mechanisms examined in this work help to provide basic understanding of brittle and ductile failure in fibrous networks. Brittle cracking occurred in gelatin electrospun scaffolds. During brittle cracking, originally random gelatin scaffolds remained random in the vicinity of the crack tip (Fig. 4). This suggests that gelatin fibers started to rupture without significant network realignment. As a result, the crack not only started propagating at small strain, but also propagated quickly.

Ductile failure occurred in PCL electrospun scaffolds and in nonwoven fabrics. During ductile failure, a blunted notch allowed for extensive deformation ahead of the notch tip prior to failure. The detailed examination of toughening mechanisms at a microscopic scale shows that fibers rearranged to become parallel bundles ahead of the notch (Figs. 5 and 6). The formation of this large number of parallel fiber bundles is the key toughening feature observed here in ductile fibrous materials. This feature toughens the fibrous scaffolds in two ways. First, the formation of fiber bundles dissipates energy by network rearrangement and thus increases input energy to failure. Second, the formation of fiber bundles at the notch tip provides a variation in the material properties, leading to a strong local material resistance against the crack.

In ductile fibrous materials, the change in the material resistance to cracking can be identified by studying the network morphology change in the vicinity of the crack tip. The parameters to quantify the microstructural morphology include (1) the angle of preferred fiber direction, (2) the dispersion about the preferred fiber direction, (3) the fiber density and (4) the fiber diameter. These parameters are crucial for determining the non-linear mechanical properties of fibrous materials [2,3,7,18,25,26,28]. The preferred direction of network alignment is perpendicular to the notch tip

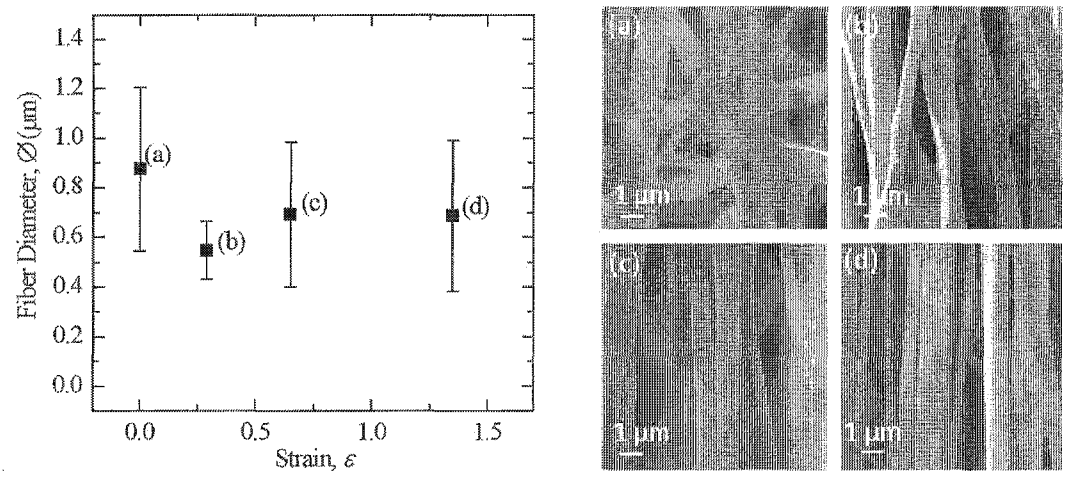

Fig. 9. The quantitative analysis of fiber diameter corresponding to increasing strains. (a–d) SEM images of the fiber bundles at the notch tips of PCL electrospun scaffolds were obtained by the novel sample-taping technique.

and parallel to the loading direction, not only accommodating the applied deformation, but also increasing the material resistance to crack propagation.

4.3. Microstructural features

Two types of electrospun scaffolds were studied here, gelatin and PCL. Both these scaffolds were produced by the sample electrospinning technique, but they exhibit two distinctive failure mechanisms. The microstructural features that differ in comparing gelatin and PCL networks include fiber stiffness, toughness, diameter, undulation and fiber density.

One of the explanations for the brittle failure observed in the gelatin network is small fiber toughness. The observation of random networks both before and after crack propagation suggests that it is easier to break the fibers than to reorient the network. Improvements in gelatin scaffolds toughness can result from spinning copolymers of gelatin and PCL [11,12]. The toughness of these copolymer scaffolds is most likely enhanced because of improved toughness of the copolymer material itself compared with that of gelatin alone.

While fiber toughness is crucial in influencing failure, the flexibility of network rearrangement around the crack tip can also determine the failure mechanism. A flexible network can allow for network rearrangement in the vicinity of the notch without resulting in large strain on the individual fibers. The flexibility of network rearrangement around the crack tip depends on a combination of factors, including fiber stiffness, fiber undulation, fiber density and bonding among fibers. An open question remains about the relative contributions to fracture toughness of these factors in electrospun materials. Such understanding requires future additional work in the form of computational parametric studies. Computational modeling that considers network architecture at a microscopic scale shows promise in explaining non-linear deformation in the vicinity of crack tip. For instance, recent finite element studies of fibrous networks suggest that partial bonding between fibers can enhance network flexibility around a notch tip [14,15].

4.4. Comparisons with other networks

Tough electrospun scaffolds can be compared with engineering polymers. Polymers have two material length scales: polymer chains at the molecular scale and bulk material at the macroscopic scale. Fibrous scaffolds as presented in this paper contain an additional hierarchical structure level: that of fibrous networks at a microscopic scale. This work demonstrates that toughening occurred at this intermediate length scale, and details how the mechanism at this level improves the material toughness. The toughening of bulk polymers involves a crazing process, as illustrated in Fig. 7. During crazing, polymer chains straighten in front of the notch tip prior to cracking [29]. As a result, more fracture energy is needed to propagate a crack. Similar to crazing in polymers, the fibers here stretched and formed a heterogeneous region in front of the notch tip in fibrous scaffolds. However, unlike crazing, no microscopic void, which can degenerate into a propagated crack [30], formed in the fibrous scaffolds. Further, fiber bundles formed not only at notch tip in fibrous scaffolds, but also across the entire region ahead of the notch tip.

The toughening mechanisms presented here are also crucial for the understanding of toughening mechanisms for natural biological tissues. Unlike the scaffolds investigated here, natural tissues consist of complex microstructures, i.e. structural fibrous networks embedded in hydrated ground substance. It is difficult to understand the more complex behavior resulting from interactions between fibrous networks and ground substance without first understanding how each component behaves individually. Therefore, this study provides a detailed basic physical understanding of the mechanics of fibrous networks by artificially excluding the gel-like ground substance that is present in a more complex biological material.

5. Conclusions

Electrospinning has emerged as a leading technique for producing tissue engineering scaffolds, owing to its ability to mimic random fibrous networks on the order of nanometers found in natural collagenous soft tissues. Both brittle and ductile failure has been demonstrated here in electrospun scaffolds. Brittle cracking in gelatin scaffolds illustrated poor toughness, leading to material failure. In contrast, toughening mechanisms in PCL scaffolds provide inspiration for the design of tough fibrous materials. The detailed examination of tough fibrous scaffolds at microscopic scales demonstrates that fibers reorientate and form fiber bundles. A large number of fiber bundles, across large regions ahead of the notch front, formed prior to crack propagation. For those fibrous networks that are unable to form fiber bundles, there is brittle cracking and correspondingly poor toughness. An understanding of

failure mechanisms demonstrates the importance of the intermediate microstructural hierarchical scale in governing fibrous material toughness. Future work will involve computational parametric studies on the relative contribution of material parameters, including fiber properties, fiber diameter and fiber density, in governing fibrous network failure. This can not only lead to useful guidelines for robust production of tissue engineering scaffolds, but also inspire the production of new engineering materials with enhanced toughness.

Acknowledgements

The authors acknowledge the Ministry of Higher Education Malaysia and the Cambridge Commonwealth Trust for funding support, Dr. Michael Sutcliffe for providing the nonwoven fabric, Anne Bahnweg for the support in the scanning electron microscope visualization, Alan Heaver for making the custom-built tensile test device used in the in situ testing, and Prof. Vikram S. Deshpande for helpful discussion.

Appendix A. Figures with essential colour discrimination

Certain figures in this article, particularly Figs. 1–3 and 6–8, are difficult to interpret in black and white. The full colour images can be found in the on-line version, at http://dx.doi.org/10.1016/j.actbio.2013.02.046.

References

[2] Nerurkar NL, Elliott DM, Mauck RL. Mechanics of oriented electrospun nanofibrous scaffolds for annulus fibrosus tissue engineering. J Orthop Res 2007;25(8):1018–28.
[3] Cortes DH, Lake SP, Kadlowec JA, Soslowsky LJ, Elliott DM. Characterizing the mechanical contribution of fiber angular distribution in connective tissue: comparison of two modeling approaches. Biomech Model Mechanobiol 2011;9(5):651–8.
[4] Vaz CM, van Tuijl S, Bouten CVC, Baaijens FPT. Design of scaffolds for blood vessel tissue engineering using a multi-layering electrospinning technique. Acta Biomater 2005 Sep;1(5):575–82.
[5] Oyen ML, Cook RF, Stylianopoulos T, Barocas VH, Calvin SE, Landers DV. Uniaxial and biaxial mechanical behavior of human amnion. J Mater Res 2005;20(11):2902–9.
[6] Hatami H, Picu RC. Effect of fiber orientation on the non-affine deformation of random fiber networks. Acta Mech 2009;84:77–84.
[7] Stachewicz U, Peker I, Tu W, Barber AH. Stress delocalization in crack tolerant electrospun nanofiber networks. ACS Appl Mater & Interfaces 2011 Jun 22;3(6):1991–6.
[8] Onck PR, Koeman T, Dillen T, Giessen E. Alternative explanation of stiffening in cross-linked semiflexible networks. Phys Rev Lett 2005;95(17):178102.
[9] Hu JJ, Chao WC, Lee PY, Huang CH. Construction and characterization of an electrospun tubular scaffold for small-diameter tissue-engineered vascular grafts: a scaffold membrane approach. J Mech Behav Biomed Mater 2012 Apr 25;13C:140–55.
[10] Stella JA, D'Amore A, Wagner WR, Sacks MS. Review on the biomechanical function of scaffolds for engineering load-bearing soft tissues. Acta Biomater 2010;6:2365–81.
[11] Zhang Y, Ouyang H, Lim CT, Ramakrishna S, Huang Z-M. Electrospinning of gelatin fibers and gelatin/PCL composite fibrous scaffolds. J Biomed Mater Res Part B Appl Biomater 2005;72(1):156–65.
[12] Lee J, Tae G, Kim YH, Park IS, Kim S-H, Kim SH. The effect of gelatin incorporation into electrospun poly(L-lactide-co-epsilon-caprolactone) fibers on mechanical properties and cytocompatibility. Biomaterials 2008 Apr;29(12):1872–9.
[14] Koh CT, Oyen ML. Branching toughens fibrous networks. J Mech Behav Biomed Mater 2012;12:74–82.
[15] Koh CT, Oyen ML. Fracture toughness of fibrous membranes. Technische Mechanik 2012;32(2–5):333–41.
[16] Sacks MS, Chuong CJ. Orthotropic mechanical properties of chemically treated bovine pericardium. Ann Biomed Eng 1998;26(5):892–902.
[17] Sacks MS. Incorporation of experimentally-derived fiber orientation into a structural constitutive model for planar collagenous tissues. J Biomech Eng 2003;125(2):280–7.
[18] Schriefl AJ, Zeindlinger G, Pierce DM, Regitnig P, Holzapfel GA. Determination of the layer-specific distributed collagen fibre orientations in human thoracic and abdominal aortas and common iliac arteries. J R Soc Interface 2012;9:1275–86.
[19] Sun X, Jeon JH, Blendell J, Akkus O. Visualization of a phantom post-yield deformation process in cortical bone. J Biomech 2010;43(10):1989–96.
[20] Song J-H, Kim H-E, Kim H-W. Production of electrospun gelatin nanofiber by water-based co-solvent approach. J Mater Sci Mater Med 2008 Jan;19(1):95–102.
[21] Li WJ, Danielson KG, Alexander PG, Tuan RS. Biological response of chondrocytes cultured in three-dimensional nanofibrous poly(epsilon-caprolactone) scaffolds. J Biomed Mater Res 2003;67(4):1105–14.
[22] NIH. available at <http://www.rsbweb.nih.gov/ij/>.
[23] Schneider CA, Rasband WS, Eliceiri KW. NIH Image to ImageJ: 25 years of image analysis. Nat Methods 2012;9(7):671–5.
[25] Gouget CLM, Girard MJ, Ethier CR. A constrained von Mises distribution to describe fiber organization in thin soft tissues. Biomech Model Mechanobiol 2012;11:475–82.
[26] Baaijens F, Bouten C, Driessen N. Modeling collagen remodeling. J Biomech 2010;43:166–75.
[28] Schriefl AJ, Reinisch AJ, Sankaran S, Pierce DM, Holzapfel GA. Quantitative assessment of collagen fibre orientations from two-dimensional images of soft biological tissues. J R Soc Interface 2012;9(76):3081–93.
[29] Deblieck RAC, Van Beek DJM, Remerie K, Ward IM. Failure mechanisms in polyolefines: the role of crazing, shear yielding and the entanglement network. Polymer 2011 Jun;52:2979–90.
[30] Powell PC. Engineering with polymers. London: Chapman & Hall; 1983. p. 120.